NASA TECHNICAL NOTE

NASA TN D-3759

NASA TN D-3759

ANALYSIS OF TEST TIMES AND BOUNDARY LAYER INDUCED PROPERTY VARIATIONS IN A CIRCULAR SHOCK TUBE

by John J. Bertin

Manned Spacecraft Center
Houston, Texas

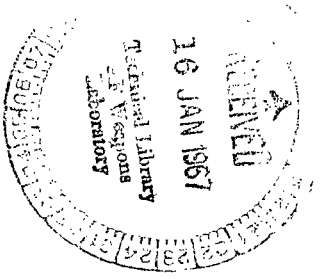

NATIONAL AERONAUTICS AND SPACE ADMINISTRATION • WASHINGTON, D. C. • JANUARY 1967

NASA TN D-3759

ANALYSIS OF TEST TIMES AND BOUNDARY LAYER INDUCED PROPERTY VARIATIONS IN A CIRCULAR SHOCK TUBE

By John J. Bertin

Manned Spacecraft Center
Houston, Texas

NATIONAL AERONAUTICS AND SPACE ADMINISTRATION

For sale by the Clearinghouse for Federal Scientific and Technical Information
Springfield, Virginia 22151 – Price $1.00

ABSTRACT

The flow field between the shock wave and the contact surface in a circular shock tube has been solved in the steady-state case, that is, one in which the contact surface moves at the same speed as the shock wave. Axial and radial variations in the velocity and thermodynamic properties due to the presence of a laminar boundary layer have been considered. The momentum and energy equations are solved simultaneously subject to the requirement that the mass flux across a given cross section of the tube equals the mass flux across the shock wave. Flow in the inviscid region is assumed to be an isentropic compression of real air.

The computed solutions were compared with measurements reported in the literature for shock Mach numbers from 4.51 to 9.50. The theoretical results are in good agreement with the measurements of the test time, the velocity profile, and the axial distribution of density.

Furthermore, the solution technique has been used to solve for the test time assuming that the boundary layer is wholly turbulent. The results indicate that boundary layer turbulence significantly reduces the test time.

ANALYSIS OF TEST TIMES AND BOUNDARY LAYER INDUCED PROPERTY VARIATIONS IN A CIRCULAR SHOCK TUBE

By John J. Bertin
Manned Spacecraft Center

SUMMARY

The flow field between the shock wave and the contact surface in a circular shock tube has been solved in the steady-state case, that is, one in which the contact surface moves at the same speed as the shock wave. Axial and radial variations in the velocity and thermodynamic properties due to the presence of a laminar boundary layer have been considered. The momentum and energy equations are solved simultaneously subject to the requirement that the mass flux across a given cross section of the tube equals the mass flux across the shock wave. Flow in the inviscid region is assumed to be an isentropic compression of real air.

The computed solutions were compared with measurements reported in the literature for shock Mach numbers from 4.51 to 9.50. The theoretical results are in good agreement with the measurements of the test time, the velocity profile, and the axial distribution of density.

Furthermore, the solution technique has been used to solve for the test time assuming that the boundary layer is wholly turbulent. The results indicate that boundary layer turbulence significantly reduces the test time.

INTRODUCTION

In an ideal shock tube, that is, one in which boundary layer and diaphragm effects are neglected, the shock wave moves at a constant velocity, and the contact surface moves at a constant, but slower velocity. Thus, for given flow conditions, the time between the passage of the shock wave and the contact surface, that is, the test time, increases linearly with the distance from the diaphragm location. Due in part to boundary layer induced acceleration of the contact surface, the experimentally observed test times are significantly shorter than the theoretical values (ref. 1). Measurements made in a low-pressure shock tube indicated the test time is independent of tube length over a tenfold range of length for all but the shortest length (ref. 2).

Early solutions for the shock-tube boundary layer were for a thin, laminar boundary layer in a perfect gas (ref. 3). The solutions were extended to include turbulent boundary layers (ref. 4), and later to incorporate real gas effects (ref. 5). A recent

study (ref. 6) considers the mutual interaction between the boundary layer and the free-stream flow. The free-stream nonuniformities and the boundary layer growth are approximated by series expansions. The inviscid region is assumed to behave as a perfect gas.

In the present investigation the momentum and energy equations for a laminar boundary layer are solved simultaneously subject to the requirement that mass flux across a given cross section of the tube equals the mass flux across the shock wave. Flow in the inviscid region is assumed to be an isentropic compression of real air. Axial and radial distribution of the velocity and thermodynamic properties are computed without a priori assumptions regarding property distributions in the shocked gas. The present paper includes shock Mach numbers from 4.5 to 9.5 and discusses the influence of turbulent boundary layers.

The analysis and computations presented in this paper are part of a doctoral dissertation submitted to Rice University.

The author wishes to express his appreciation to those who contributed of their time and knowledge to this investigation: J. Kenneth Oney of Lockheed Electronics Corp. for invaluable programing assistance and advice, and Dr. F. A. Wierum of Rice University and K. C. Weston of MSC for enlightening discussions.

SYMBOLS

a	speed of sound, ft/sec
C	Chapman-Rubesin factor, $\frac{\rho\mu}{\rho_w\mu_w}$
c_p	specific heat, Btu/slug-°R
f	reduced stream function, equation (6)
g	reduced enthalpy function, H/H_{se}
H	total enthalpy in shock-fixed coordinate system, $h + \frac{1}{2}u^2$, ft^2/sec^2
h	static enthalpy, ft^2/sec^2
J	mechanical equivalent of heat, 778 ft-lbf/Btu
k	thermal conductivity, Btu/ft-sec-°R
M_s	shock Mach number, U_s/a_1
P_r	Prandtl number, $P_r = \mu c_p/k$

p	static pressure, lbf/ft^2
$\dot{q}$	heat transfer rate, Btu/ft^2-sec
R	radius of shock tube, ft
r	radial distance from axis of shock tube, ft
Re_L	Reynolds number used in heat transfer correlation, defined by equation (22)
Re_{x_m}	Reynolds number used in boundary layer transition criteria, defined by equation (18)
St	Stanton number, defined by equation (21)
s	transformed x-coordinate, defined by equation (2)
T	static temperature, $^\circ R$
U	component of velocity in x-direction, laboratory fixed coordinates, ft/sec
u	component of velocity in x-direction, shock-wave fixed coordinates, ft/sec
v	component of velocity in y-direction, shock-wave fixed coordinates, ft/sec
x	axial distance in shock-wave fixed coordinates, measured from shock wave, ft
e_{eq}	equivalent length, ft
x_m	axial distance from shock wave to contact surface from viscous solution, ft
y	coordinate normal to wall, ft
β	dimensionless test parameter defined by equation (17)
δ	boundary layer thickness defined by y-coordinate where $U = 0.99U_e$, ft
ϵ	density ratio, ρ_2/ρ_1
η	transformed y-coordinate, defined by equation (3)
θ	dimensionless density, $\frac{\rho}{\rho_w}$
μ	dynamic viscosity, $lbf\text{-}sec/ft^2$

ν kinematic viscosity, ft^2/sec

ρ density, $slugs/ft^3$

$\bar{\rho}$ density, averaged over cross section of tube, $slugs/ft^3$

τ test time, sec

ψ stream function, defined by equation (6)

Subscripts:

aw adiabatic wall

e conditions evaluated at edge of boundary layer

eo conditions evaluated in inviscid region just downstream of shock wave

s conditions for shock wave

se stagnation conditions in inviscid portion of flow

w conditions evaluated at wall

wo conditions evaluated at wall just downstream of shock wave

1 conditions evaluated upstream of shock wave

ANALYSIS

It has been observed that the test time in a shock tube reaches a limiting value due to the growth of a boundary layer. In this limiting case, Duff (ref. 2) concluded that the contact surface moves at the same speed as the shock wave. The test gas passing through the shock wave is removed through the boundary layer at the contact surface. In a shock-wave fixed coordinate system, the problem is a steady-state one, as shown in figure 1.

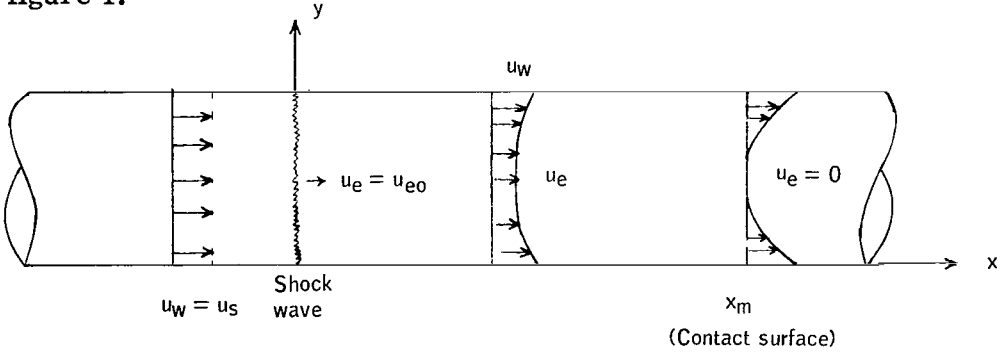

Figure 1.- Test gas flow field in shock-wave fixed coordinate system.

For a laminar boundary layer, assumed to be in thermodynamic equilibrium with a Lewis number of 1, the equations of motion are

$$\frac{\partial(\rho u)}{\partial x} + \frac{\partial(\rho v)}{\partial y} = 0 \tag{1a}$$

$$\rho u \frac{\partial u}{\partial x} + \rho v \frac{\partial u}{\partial y} = - \frac{\partial p}{\partial x} + \frac{\partial}{\partial y}\left(\mu \frac{\partial u}{\partial y}\right) \tag{1b}$$

$$\rho u \frac{\partial H}{\partial x} + \rho v \frac{\partial H}{\partial y} = \frac{\partial}{\partial y}\left(\frac{\mu}{P_r} \frac{\partial H}{\partial y}\right) + \frac{\partial}{\partial y}\left[\frac{\mu}{2}\left(1 - \frac{1}{P_r}\right)\frac{\partial\left(u^2\right)}{\partial y}\right] \tag{1c}$$

Making the standard boundary layer assumption that

$$\frac{\partial p}{\partial y} = 0$$

and the pressure gradient, from the inviscid momentum equation, is

$$\frac{\partial p}{\partial x} = \frac{dp}{dx} = - \rho_e u_e \frac{du_e}{dx}$$

then the momentum equation becomes

$$\rho u \frac{\partial u}{\partial x} + \rho v \frac{\partial u}{\partial y} = \rho_e u_e \frac{du_e}{dx} + \frac{\partial}{\partial y}\left(\mu \frac{\partial u}{\partial y}\right) \tag{1d}$$

Ordinarily in the case of two-dimensional flow, the equations of motion, which are nonlinear partial differential equations, are reduced to a pair of ordinary, nonlinear differential equations by means of a coordinate transform which automatically satisfies the continuity equation. A commonly used transform is that of Levy (ref. 7) as modified by Lees (ref. 8). This "Levy-Lees" transformation makes use of the velocity, density, and viscosity evaluated at the edge of the boundary layer. Since the inviscid velocity, which is a function of x, goes to zero at the contact surface of the shock-wave fixed coordinate system, this transformation was considered unsatisfactory

for the present problem. The following modified form of the Levy-Lees transformation was used:

$$s = \int_0^x \rho_w \mu_w u_w \, dx \tag{2}$$

$$\eta = \frac{\rho_w u_w}{(2s)^{1/2}} \int_0^y \frac{\rho}{\rho_w} \, dy \tag{3}$$

Thus, the differential operators become

$$\left(\frac{\partial}{\partial y}\right)_x = \frac{\rho u_w}{(2s)^{1/2}} \left(\frac{\partial}{\partial \eta}\right)_s \tag{4}$$

$$\left(\frac{\partial}{\partial x}\right)_y = \rho_w \mu_w u_w \left[\left(\frac{\partial \eta}{\partial s}\right)_y \left(\frac{\partial}{\partial \eta}\right)_s + \left(\frac{\partial}{\partial s}\right)_\eta\right] \tag{5}$$

A stream function ψ is defined such that the continuity equation is satisfied automatically

$$\rho u = \frac{\partial \psi}{\partial y}$$

$$\rho v = -\frac{\partial \psi}{\partial x}$$

Solving for the stream function

$$\psi = (2s)^{1/2} \int \frac{u}{u_w} \, d\eta = (2s)^{1/2} \, f(\eta) \tag{6}$$

Thus,

$$\frac{u}{u_w} = \left(\frac{\partial f}{\partial \eta}\right)_s \tag{7}$$

Substituting equations (2) to (7) into the momentum and energy equations yields

$$f\left(\frac{\partial^2 f}{\partial \eta^2}\right)_s + \frac{\partial}{\partial \eta}\left(\frac{\rho\mu}{\rho_w \mu_w}\frac{\partial^2 f}{\partial \eta^2}\right)_s + 2s\frac{\rho_e u_e}{\rho_w u_w^2}\frac{du_e}{ds} = 2s\left\{\left(\frac{\partial f}{\partial \eta}\right)_s\left[\frac{\partial\left(\frac{\partial f}{\partial \eta}\right)_s}{\partial s}\right]_y - \left(\frac{\partial^2 f}{\partial \eta^2}\right)_s\left(\frac{\partial f}{\partial s}\right)_y\right\} \tag{8}$$

and

$$f\left(\frac{\partial g}{\partial \eta}\right)_s + \frac{\partial}{\partial \eta}\left[\frac{\rho\mu}{\rho_w \mu_w}\frac{1}{P_r}\left(\frac{\partial g}{\partial \eta}\right)_s\right]_s + \frac{u_w^2}{H_{se}}\frac{\partial}{\partial \eta}\left[\frac{\rho\mu}{\rho_w \mu_w}\left(1 - \frac{1}{P_r}\right)\left(\frac{\partial f}{\partial \eta}\right)_s\left(\frac{\partial^2 f}{\partial \eta^2}\right)_s\right]$$

$$= 2s\left[\left(\frac{\partial f}{\partial \eta}\right)_s\left(\frac{\partial g}{\partial s}\right)_y - \left(\frac{\partial g}{\partial \eta}\right)_s\left(\frac{\partial f}{\partial s}\right)_y\right] \tag{9}$$

where

$$g = \frac{H}{H_{se}}$$

Assuming local similarity holds for the velocity and the enthalpy profiles (ref. 9), the terms on the right-hand side of equations (8) and (9) may be neglected. Thus, the following forms for the equations for conservation of momentum and energy are obtained

$$ff'' + (Cf'')' + \frac{2s}{\theta}\frac{\rho_e u_e}{\rho_w u_w^2}\frac{du_e}{ds} = 0 \tag{10}$$

$$fg' + \left(\frac{c}{P_r}g'\right)' + \frac{u_w^2}{H_{se}}\left(1 - \frac{1}{P_r}\right)(Cf'f'')' = 0 \tag{11}$$

In equations (10) and (11), the prime denotes differentiation with respect to η, and

$$\theta = \frac{\rho}{\rho_w}$$

$$C = \frac{\rho\mu}{\rho_w \mu_w}$$

Furthermore, the Prandtl number has been assumed to be constant.

The boundary conditions for the momentum and energy equations at the wall are

$$f(0) = 0 \tag{12a}$$

$$f'(0) = 1 \tag{12b}$$

$$g(0) = g_w = 1 \tag{12c}$$

and at the edge of the boundary layer are

$$f'(\infty) = \frac{u_e}{u_w} = \text{function(s)} \tag{12d}$$

$$g(\infty) = 1 \tag{12e}$$

Implicit in the boundary conditions is the assumption that the wall temperature is constant (and equal to the static temperature ahead of the shock). Measurements made by Martin (ref. 10) support the assumption of constant wall temperature.

In addition to the momentum and the energy equation, flow in the shock tube must satisfy the overall continuity equation

$$\rho_{eo}\, U_{eo}\, \pi R^2 = \rho_e\, U_e\, \pi R^2 + \int_0^R \left(\rho u - \rho_e\, u_e\right) 2\pi r\, dr$$

Transforming the preceding equation into the current notation so that the variables are the same as those used in the momentum and the energy equations, the continuity equation becomes

$$\rho_{eo}\, u_{eo} = \rho_e\, u_e + \frac{2(2s)^{1/2}}{R}\int_0^{\infty}\left(\theta f' - \frac{\rho_e u_e}{\rho_w u_w}\right)\left(1 - \frac{(2s)^{1/2}}{\rho_w u_w}\frac{\int_0^{\eta}\frac{d\eta}{\theta}}{R}\right)\frac{d\eta}{\theta} \qquad (13)$$

To facilitate numerical solution of equations (10) to (13), the dimensionless parameters θ and C must be expressed as a function of f and g. The thermodynamic charts of reference 11 are used to calculate the density ratio and the temperature ratio for a given wall temperature over a range of pressure. The viscosity is calculated using Sutherland's relation for air

$$\mu = 2.28 \times 10^{-7}\,\frac{T^{3/2}}{T + 199}$$

modified at high temperatures by the factors of reference 12. The results are virtually independent of pressure for the range of pressures considered in this report.

The equations of Mirels (ref. 5) provide a satisfactory correlation of the calculations. The expression used for Chapman-Rubesin factor C is

$$C = \frac{1.5481}{\sqrt{\frac{h}{h_w}}} - \frac{0.5481}{\frac{h}{h_w}} + 0.0028\left(\frac{h}{h_w} - 1\right) - 5.74 \times 10^{-5}\left(\frac{h}{h_w} - 1\right)^2 \qquad (14)$$

The values computed using equation (14) are within 3 percent of the values calculated using the thermodynamic charts together with Sutherland's viscosity. Similarly, θ can be approximated by the relation

$$\theta = \frac{0.02586\,\frac{h}{h_w} + 0.94828}{\frac{h}{h_w} - 0.02586} \qquad (15)$$

Although equation (15) is correct to within a few percent for the majority of the pressure and enthalpy range of interest, the values obtained using equation (15) differ by as much as 22 percent from the calculations based on the thermodynamic charts at the highest enthalpies and the lowest pressures considered in this report.

In equations (14) and (15)

$$\frac{h}{h_w} = \frac{g - \frac{u_w^2}{2H_{se}} (f')^2}{\frac{h_w}{H_{se}}} \tag{16}$$

Thus, equations (10), (11), and (13) constitute the system of equations governing test gas flow in a shock tube. When supplemented by the assumption that flow in the inviscid portion of the shock tube is isentropic and by an equation of state, the equations may be solved to give the flow field of the shocked gas subject to the boundary conditions outlined in equation (12).

DISCUSSION

Laminar Flow

The flow field of shock-compressed gas in a circular shock tube has been solved for the steady-state case, for which the test time has reached its maximum value. Consideration has been given to variations in the inviscid properties due to the presence of a laminar boundary layer. The momentum and energy equations are solved simultaneously subject to the requirement that, in the steady-state problem, the mass flux of shocked gas across any cross section is equal to the mass flux across the shock wave. The solution of the equations is repeated at locations further downstream of the shock until all the mass flux is contained in the boundary layer, that is, the edge velocity in shock-wave fixed coordinates goes to zero. This model is consistent with experimental observations, in which the contact surface and the shock wave move with the same speed.

Test times were computed by direct solutions of equations (10), (11), and (13) accounting for the velocity gradient term. The test times were also computed neglecting the velocity gradient. A compilation of the computed test times is presented in table I. Solutions neglecting the velocity gradient gave test times virtually identical to those computed accounting for the velocity gradient. The effect of the radius on the theoretical test time was checked. For $M_s = 7.59$ and $p_1 = 2.78$ psf, flow-field solutions neglecting the velocity gradient were obtained for three different shock-tube diameters. The test time is proportional to the square of the radius.

TABLE I. - TEST TIMES COMPUTED FOR SHOCK WAVE

MOVING AT HYPERSONIC SPEED

M_s	p_1, lbf/ft^2	R, ft	β	τ, μsec	x_m, ft	Velocity gradient
9.50	0.556	0.08333	1.141	20.81	0.2208	zero
9.50	.556	.08333	1.141	20.81	.2208	nonzero
7.62	.556	.08333	1.251	28.36	.2417	zero
7.59	.278	.04688	1.244	4.336	.0375	zero
7.59	.278	.08333	1.254	13.49	.1167	zero
7.59	.278	.12083	1.248	28.64	.2477	zero
7.59	.278	.12083	1.248	28.64	.2477	nonzero
6.67	2.78	.08333	1.328	172.1	1.2833	zero
6.28	.806	.12083	1.395	109.6	.7710	zero
5.905	2.78	.08333	1.396	207.0	1.3667	zero
5.90	1.751	.12083	1.368	262.7	1.8125	zero
5.00	.556	.07375	1.430	38.09	.2131	zero
5.00	.556	.07375	1.425	38.60	.2158	nonzero
5.00	2.78	.07375	1.464	221.6	1.2390	zero
5.00	13.90	.07375	1.468	1134.6	6.3425	zero
5.00	13.90	.07375	1.464	1134.6	6.3425	nonzero

The computed test times are presented in figure 2 in terms of the dimensionless test parameter β as a function of the shock Mach number. The parameter β is given by the relation

$$\beta^2 = \frac{R^2}{4x_m}\left(\frac{\rho_{eo}}{\rho_{wo}}\right)^2\left(\frac{u_{eo}}{u_w - u_{eo}}\right)\frac{u_{eo}}{\nu_{wo}} \tag{17}$$

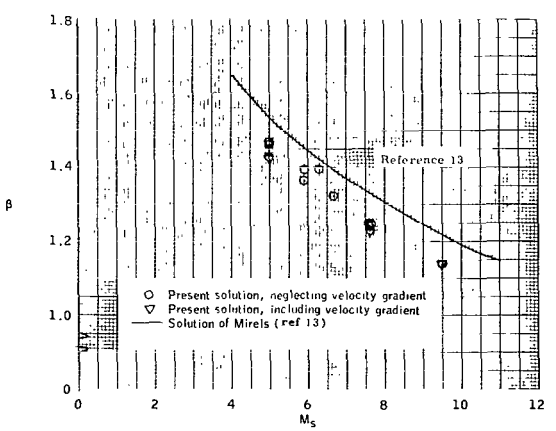

Figure 2.- Values of β as a function of M_s.

For hypersonic shock waves, that is, M_s greater than 5, β was virtually unaffected by the velocity gradient. At a given shock Mach number, variations in the diameter or in the static pressure upstream of the shock wave resulted in only slight variations in β. Included for comparison is the relation found by Mirels (ref. 13) assuming a thin boundary layer. In general, the present solution provides values of β which are 5 to 10 percent less than the values of Mirels.

The computed test times are compared with the experimental values of Roshko (ref. 14), Bray (ref. 15), and Sandborn (ref. 16) in table II. No distinction is made between the flow-field solutions accounting for the velocity gradient and those neglecting it, since the test time was virtually independent of the velocity gradient term at these conditions. The theoretical test time exceeds the measurements by more than 10 percent in half of the cases investigated. The discrepancy is attributed to turbulent mixing across the contact surface and to turbulence in the boundary layer. A Reynolds number, similar to that used in reference 17 to correlate experimental data, was defined as

$$Re_{x_m} = \rho_{eo} \frac{\left(u_w - u_{eo}\right)^2}{\mu_{eo}} \frac{x_m}{u_{eo}} \tag{18}$$

TABLE II. - COMPARISON OF MEASURED AND THEORETICAL TEST TIMES

M_s	p_1, lbf/ft^2	τ (computed), μsec	τ (measured), μsec	Source	$Re_{x_m} \times 10^{-5}$
9.50	0.556	20.81	18.8	Roshko	0.67
7.62	.556	28.36	36	Roshko	.41
7.59	.278	28.64	20 to 35	Sandborn	.20
6.67	.278	172.1	131.5	Roshko	7.15
6.28	.806	109.6	80 to 100	Sandborn	1.05
5.905	2.78	207.0	109	Roshko	5.71
5.90	1.751	262.7	170 ± 30	Sandborn	5.24
5.00	.556	38.09	38	Bray	.20
5.00	2.78	221.6	89	Bray	3.88
5.00	13.90	1134.6	144	Bray	9.35

In each case where the computed test time significantly exceeds the measured value, the Reynolds number is greater than 3.5×10^5. The Reynolds number is reasonably close to the transition criteria indicated by the data of reference 17, which was a transition Reynolds number of 5.0×10^5. Thus, turbulence in the boundary layer is assumed to be a major source of the discrepancy between measurements and theory.

For a shock wave moving at hypersonic speed, the computed test time is a function of the static pressure upstream of the shock, the radius of the shock tube, and the

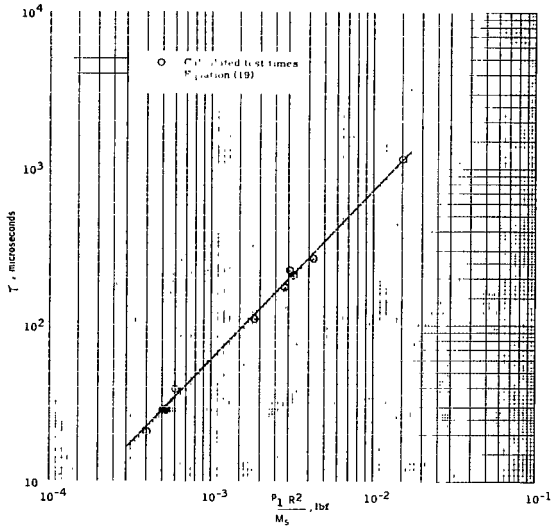

Figure 3.- Correlation of the computed test times.

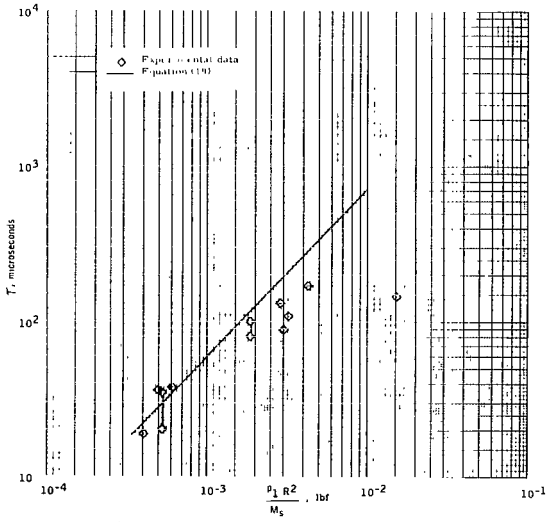

Figure 4.- Comparison of measured and theoretical test times, laminar flow.

shock Mach number. As indicated in figure 3, the computed test times are closely approximated by the equation

$$\tau = 1.06 \times 10^5 \left(\frac{p_1 R^2}{M_s} \right)^{1.088} \qquad (19)$$

The use of $\frac{p_1 R^2}{M_s}$ as a correlating parameter has been suggested by Roshko.

The experimentally-determined test times are presented in figure 4 as discrete values or as a range of values, depending on the data reported. The measurements are in good agreement with equation (19) for a value of $\frac{p_1 R^2}{M_s}$ less than 0.002 pound. At higher values of the correlating parameter, the experimental test times are significantly less than the computed values. As discussed previously, boundary layer turbulence is considered to be a prime contributor to this discrepancy.

The change in the density, averaged over the cross section, is presented in figure 5 as a function of the square root of the distance from the shock wave. The density distribution is from the flow-field solution for $M_s = 7.59$ and $p_1 = 0.278$ psf. The solution includes the effect of the velocity gradient term. As was observed experimentally by Duff (ref. 2), the fractional change in the density is a linear function of the square root of the fractional distance from the shock to the contact surface.

In the steady-state problem, the shock wave and the contact surface move at the same speed. Since the contact surface is assumed to be impermeable in the inviscid region, the inviscid velocity in shock-fixed coordinates is zero at the contact surface. Thus, the inviscid velocity varies along the axis of the shock tube, decreasing from the value immediately downstream of the shock wave to zero at the contact surface. The variation exists because the fraction of the mass flux across a cross section of the shock tube which is transported by the boundary layer increases as the boundary layer grows. The local inviscid velocity relative to the velocity immediately behind the

shock is presented in figure 6 as a function of the fraction of the distance from the shock wave to the contact surface. The velocity distributions were obtained from the flow-field solutions accounting for the velocity gradient. The axial velocity distribution is seen to be independent of the flow conditions over the range of hypersonic Mach numbers investigated.

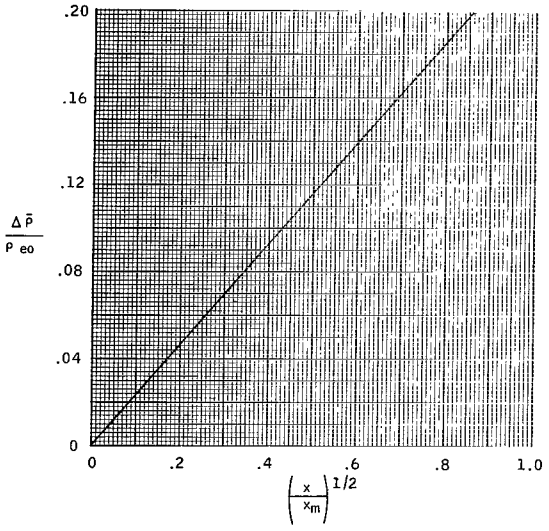

Figure 5.- Variation in average density as a function of the position in the shock tube. $M_s = 7.59$.

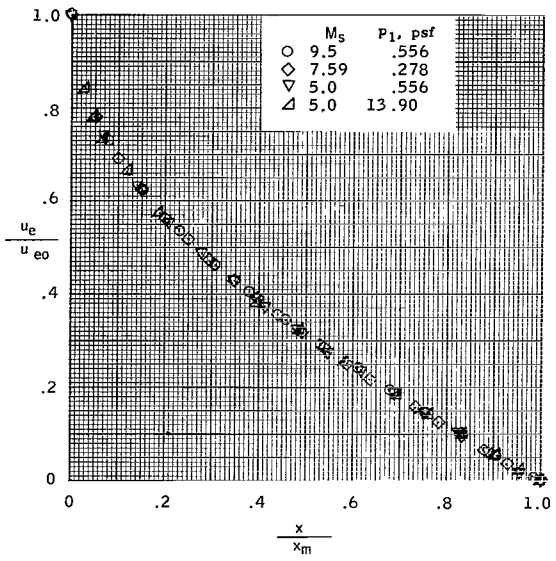

Figure 6.- Computed axial distribution of the inviscid velocity.

Once the variation of the velocity is obtained, the associated change in the thermodynamic properties can be computed if the process by which the gas is decelerated is defined. In the present solution the thermodynamic properties were computed assuming an isentropic compression of the inviscid flow in accordance with the velocity function described in figure 6. The axial distribution of pressure and enthalpy, thus computed, are presented in figures 7(a) and 7(b), respectively. Although the velocity is a function of axial position only, the pressure and the enthalpy depend upon the flow conditions as well as the location. At a given location, the fractional increase in the pressure, or enthalpy, is inversely proportional to the shock Mach number. Most of the incremental change in the thermodynamic property is accomplished in the first half of the test length. Over the last half of the test length, the

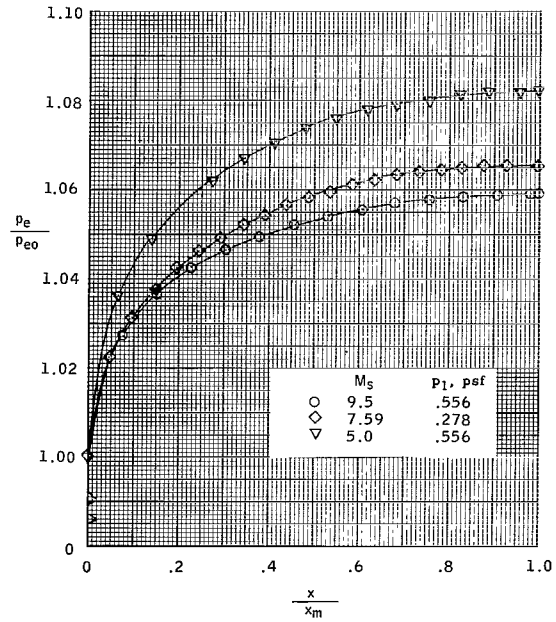

(a) Pressure

Figure 7.- Axial distribution of thermodynamic properties.

property varies relatively little, asymptotically approaching the value at the contact surface.

In addition to the computed test times and the axial distributions of the flow parameters, which have been discussed, the solution of equations (10) to (13) yields radial distributions. From the solution for $M_s = 7.59$ and $p_1 = 0.278$ psf, the boundary layer profiles at a cross section approximately one-fourth of the distance from the shock wave to the contact surface are presented in figures 8(a), 8(b), and 8(c). The boundary layer parameters are presented as a function of η, the transformed y-coordinate. For figure 8 the "edge" of the boundary layer is defined as the value of η for which $|f''| = 0.0005$. This definition was employed in the computer program instead of the more conventional definition that $U/U_e = 0.99$ at the edge.

The transformed stream function and its first and second derivatives with respect to η are presented in figure 8(a). The velocity function $f' = u/u_w$ varies

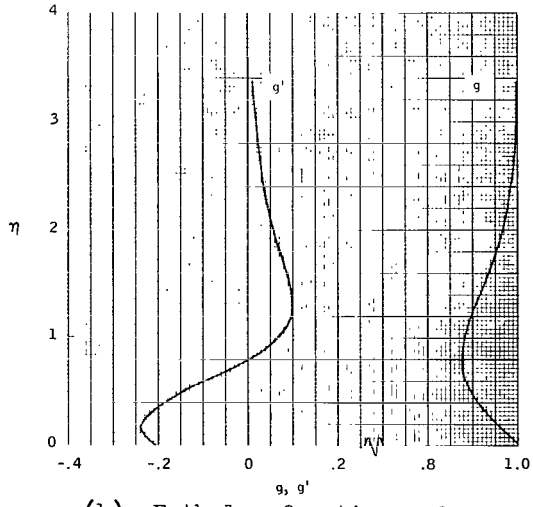

(b) Enthalpy function and derivatives.

Figure 8.- Continued.

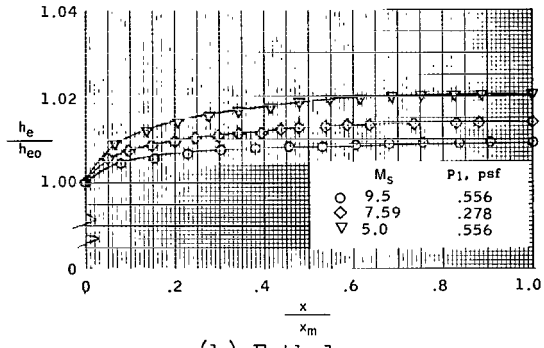

(b) Enthalpy

Figure 7.- Concluded.

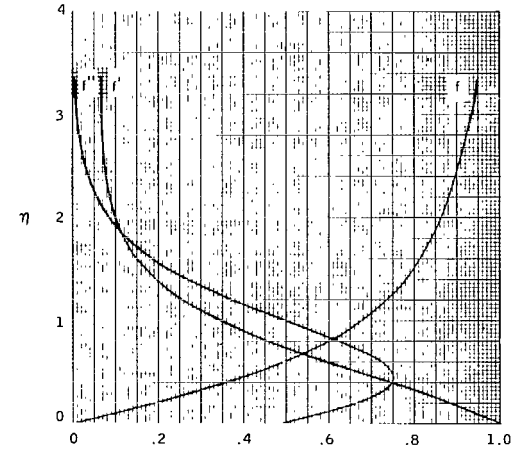

(a) Velocity function and its derivatives.

Figure 8.- Boundary layer profiles, $M_s = 7.59$, $p_1 = 0.278$ psf, $x/x_m = 0.2683$.

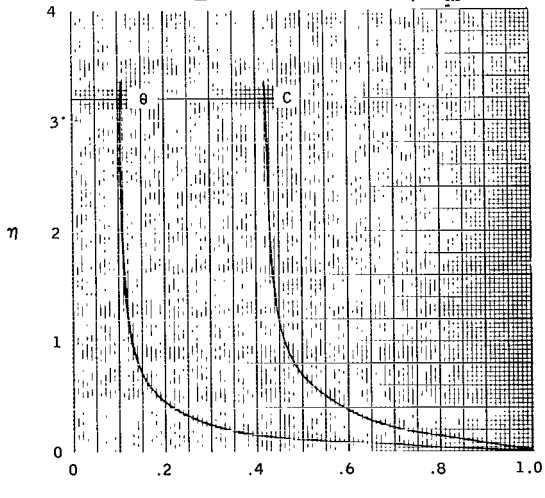

(c) Density and Chapman-Rubesin factor

Figure 8.- Concluded.

from 1 at the wall to $u_e/u_w = 0.0608$ at the boundary layer edge. In laboratory-fixed coordinates the velocity profile is given by

$$\frac{U}{U_e} = \frac{1 - f'}{1 - f'_e}$$

The shear function, which is a maximum a short distance from the wall, asymptotically approaches zero as $\eta \to \infty$.

The dimensionless enthalpy function and its first derivative with respect to η are presented in figure 8(b). In the boundary layer the total enthalpy varies from $0.87H_{se}$ to $1.0H_{se}$. The enthalpy gradient is negative at the wall, goes positive, and finally approaches zero asymptotically as $\eta \to \infty$.

The density function $\theta = \frac{\rho}{\rho_w}$ and the Chapman-Rubesin factor are presented in figure 8(c). Near the wall both parameters decrease rapidly as η increases. Furthermore, they approximate their edge values at $\eta = 1.2$ and vary little for $\eta > 1.2$.

Values of $f''(0)$ and $g'(0)$ and $\frac{\delta}{R}$ are presented in table III as a function of the inviscid flow parameters relative to their wall values and of a dimensionless axial coordinate. The computed values reflect the influence of the velocity gradient on the flow-field solution. By using these values for the shear function and the enthalpy gradient, the heat-transfer rate was computed. Substitution of the coordinate transformation, equation (4), and the definitions of f and g into the heat-transfer equation

$$\dot{q} = -\left(\frac{k}{c_p}\frac{\partial h}{\partial y}\right)_w$$

yields

$$\dot{q} = -\frac{\rho_w u_w H_{se}}{JP_r}\frac{\mu_w}{(2s)^{1/2}}\left[g'(0) - \frac{u_w^2}{H_{se}} f''(0)\right] \tag{20}$$

TABLE III. - SHEAR FUNCTION, ENTHALPY GRADIENT, AND BOUNDARY LAYER THICKNESS FROM SOLUTIONS OF FLOW FIELD FOR HYPERSONIC SHOCK WAVE

Flow conditions		$\frac{x}{x_m}$	$\frac{h_e}{h_w}$	$\frac{u_e}{u_w}$	C_e	θ_e	$f''(0)$	$g'(0)$	$\frac{\delta}{R}$
M_s	p_1, lbf/ft^2								
9.50	0.566	0.0755	18.862	0.07397	0.3591	0.07625	-0.4584	-0.2017	0.0340
		.8305	18.958	.00968	.3584	.07596	-.4755	-.2135	.1339
7.59	0.278	0.0244	12.360	0.10389	0.4202	0.1028	-0.4741	-0.1997	0.0236
		.2683	12.443	.06080	.4194	.1023	-.4894	-.2088	.0781
		.5122	12.471	.03686	.4190	.1021	-.4972	-.2137	.1111
		.7561	12.483	.01732	.4189	.1020	-.5020	-.2173	.1348
5.00	0.566	0.0173	5.894	0.13600	0.5571	0.1876	-0.5056	-0.1886	0.0222
		.1903	5.945	.09007	.5552	.1862	-.5246	-.1985	.0750
		.3633	5.964	.06512	.5545	.1857	-.5349	-.2039	.1051
		.5363	5.977	.04509	.5541	.1854	-.5417	-.2078	.1251
		.7618	5.983	.02301	.5538	.1852	-.5475	-.2118	.1660

The computed heating rates presented in terms of the Stanton number are presented in table IV as a function of the Reynolds number Re_L. The Stanton number is given by the relation

$$St = \frac{\dot{q}}{\rho_e(u_w - u_e)(h_{aw} - h_w)} \tag{21}$$

and the Reynolds number by

$$Re_L = \frac{\rho_e(u_w - u_e)x}{\mu_e} \tag{22}$$

Over the range of flow conditions considered, the product $St\sqrt{Re_L}$ is essentially constant. The measurements reported in reference 18 also indicate that this parameter is essentially constant over the shock Mach number range $(1 < M_s < 10)$ and is independent of pressure. However, the experimental values of $St\sqrt{Re_L}$, which were evaluated neglecting axial variations in the inviscid properties, are between 0.6 and 0.85. To

assess the influence of the velocity gradient term on the computed value of $St\sqrt{Re_L}$, a flow-field solution was obtained neglecting the velocity gradient term but accounting for changes in the inviscid flow. The value of $St\sqrt{Re_L}$, thus computed for $M_s = 7.59$ and $p_1 = 0.278$ psf, was 1.130, which is essentially the same as the values of table IV. Since the experimental values are from the literature, it is difficult to define possible sources of error and hence to assess discrepancies between the heat transfer measurements and the present theory.

TABLE IV. - COMPUTED HEAT TRANSFER CORRELATIONS

Flow conditions		$\frac{x}{x_m}$	St	Re_L	$St\sqrt{Re_L}$
M_s	p_1, lbf/ft^2				
9.50	0.566	0.0755 .8305	0.0474 .01504	593 6450	1.157 1.206
7.59	0.278	0.0244 .2683 .5122 .7651	0.1315 .0386 .0283 .0228	73 871 1672 2530	1.126 1.140 1.158 1.146
5.00	0.556	0.0173 .1903 .3633 .5363	0.1352 .0397 .0283 .0232	64 770 1515 2300	1.080 1.103 1.100 1.113

Turbulent Flow

The discrepancies between the experimentally observed test times and the theoretical values shown in figure 4 and table II were attributed to turbulence in the boundary layer. The conclusion was based on the Reynolds number. To further support the assumption, the test times were computed accounting, in an approximate manner, for a fully developed turbulent boundary layer originating at the shock wave.

Since, for turbulent flow, the compressible boundary layer is not much thicker than the incompressible boundary layer (ref. 18), the relations for two-dimensional, incompressible flow over a flat plate are used to describe the velocity profile and the

boundary layer growth. The velocity in laboratory-fixed coordinates is assumed to obey the $\frac{1}{7}$ th-power law, that is,

$$\frac{U}{U_e} = \left(\frac{y}{\delta}\right)^{1/7} = \frac{u_w - u}{u_w - u_e}$$

Solving for the velocity in the shock-wave fixed coordinate system yields

$$f' = \frac{u}{u_w} = 1 - \left(\frac{y}{\delta}\right)^{1/7}\left(1 - \frac{u_e}{u_w}\right) \tag{23}$$

Correspondingly, the boundary layer thickness is assumed to obey the relation for a flat plate (ref. 18).

$$\delta = 0.37\left(x_{eq}\right)^{0.8}\left(\frac{\mu e}{U_e \rho_e}\right)^{0.2} \tag{24}$$

Since the properties vary in the axial direction, the equivalent length x_{eq} is used in equation (24) instead of the physical distance from the shock wave. The equivalent length is defined as that length which, if the properties are assumed constant and equal to the values at the cross section of interest, yields a boundary layer thickness equal to the thickness calculated accounting for the property variation.

Although the velocity profiles and the boundary layer thickness are given by incompressible flow relations, solutions were obtained treating the density both (1) as a variable across the boundary layer and (2) as a constant, equal to the wall density. The expression for the variable density is

$$\theta = \frac{0.02586\,\frac{h}{h_w} + 0.94828}{\frac{h}{h_w} - 0.02586} \tag{25}$$

where

$$\frac{h}{h_w} = \frac{1 - \frac{u_w^2}{2H_{se}} (f')^2}{\frac{h_w}{H_{se}}} \tag{26}$$

Equation (26) incorporates the assumption that the total enthalpy is invariant across the boundary layer.

In addition to satisfying the above equations, flow in the shock tube must satisfy the overall continuity relation

$$\rho_{eo} u_{eo} = \rho_e u_e + \frac{2\rho_w u_w}{R^2} \int_0^\delta \left(f'\theta - f'_e \theta_e\right)(R - y)\, dy \tag{27}$$

Thus, equations (23) through (27) constitute a system of equations approximating the gas flow in a shock tube in the presence of a turbulent boundary layer. The equations are supplemented by the assumption that flow in the inviscid portion of the shock tube is isentropic and by an equation of state.

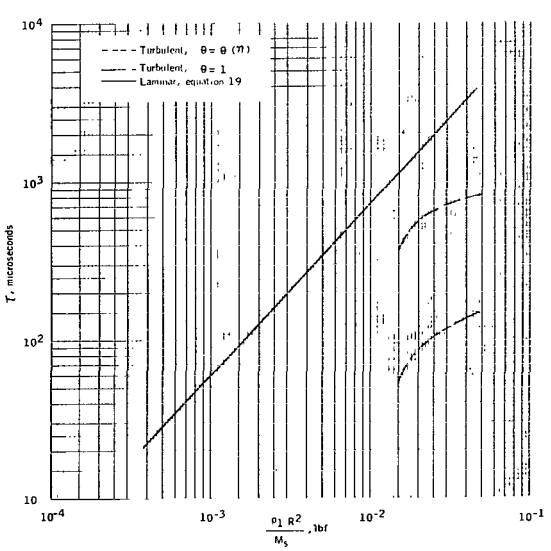

Figure 9.- Test times for a turbulent boundary layer.

The test time computations are summarized in figure 9 and in table V. As mentioned, solutions were obtained both for $\theta = 1$ and for $\theta = \theta(\eta)$. The test times computed assuming the density to be constant are almost an order of magnitude shorter than the values computed using equation (25) to define the density profile. It is believed that the present approach may be used as a framework for a more rigorous analysis of the turbulent boundary layer to provide improved flow-field solutions. Experimental measurements of the steady-state time where the boundary layer is known to be turbulent are not available for comparison with the computed times.

TABLE V.- COMPUTED TEST TIMES IN THE PRESENCE OF A TURBULENT BOUNDARY LAYER

M_s	p_1, psf	R, ft	$\theta = 1$		$\theta = \theta(\eta)$	
			β	τ, μsec	β	τ, μsec
5.00	13.90	0.07375	6.790	52.77	2.566	369.4
5.00	6.795	.12083	6.090	86.46	2.381	562.0
4.51	13.75	.12083	7.460	143.56	3.134	813.5

CONCLUDING REMARKS

The solution of the flow field between the shock wave and the contact surface in a circular shock tube has been obtained for the steady-state case, that is, one in which the shock wave and the contact surface move at the same speed. The momentum and energy equations are solved simultaneously subject to the requirement that the mass flux across a given cross section of the tube equals the mass flux across the shock wave. The boundary layer is assumed to be wholly laminar. Flow in the inviscid region is assumed to be an isentropic compression of real air.

The equations are transformed from the physical (x, y) coordinate system by means of a unique transformation which is a modification of the Levy-Lees transformation. An iterative process employing fourth order Runge-Kutta numerical integration formulas is used to solve the momentum and energy equations in the boundary layer. The boundary layer profiles and inviscid fluid properties are adjusted until the requirement of conservation of mass flux across a shock-tube cross section is satisfied.

Axial and radial variations in the velocity and thermodynamic properties are accounted for in the solution. For shock Mach numbers greater than 5, the test times are virtually independent of the velocity gradient.

The computed solutions were compared with experimental data representing shock Mach numbers from 4.5 to 9.50. The comparisons indicate that the computed flow field is a valid representation of the actual situation. Specifically, the following conclusions were reached:

(1) The change in the density, averaged over the cross section, is a linear function of the square root of the distance from the shock wave. The linear relation was experimentally observed by Duff.

(2) The flow-field solutions gave test times which are in good agreement with the experimental values, providing the measurements were made for a laminar boundary

layer. Furthermore, the test time was found to be a function of the static pressure upstream of the shock multiplied by the square of the Reynolds number and divided by the shock Mach number $\left(\frac{p_1 R^2}{M_s}\right)$, as predicted by Roshko.

(3) The computed solutions gave a constant value for a heat transfer correlation parameter $St\sqrt{Re_L}$. Although the magnitude of this parameter measured by Hartunian was significantly different, the measurements indicate that the parameter was independent of the shock Mach number and static pressure upstream of the shock as was computed theoretically. The agreement between the measurements and the computed solutions indicates the technique provides a valid description of the flow between the shock wave and the contact surface when the boundary layer is laminar. Thus, the test time and both radial and axial distributions of the velocity and thermodynamic properties can be computed without a priori assumptions regarding the shocked gas.

A major source of discrepancy between the measurements and theory is assumed to be boundary layer turbulence. Preliminary calculations indicate that the approach employed for a laminar boundary layer can be used if the proper relations governing turbulent boundary layers are used.

Manned Spacecraft Center
National Aeronautics and Space Administration
Houston, Texas, September 28, 1966
030-0000-CR-72

REFERENCES

1. Glass, I. I.; and Patterson, G. N.: A Theoretical and Experimental Study of Shock-Tube Flows. Journal of the Aeronautical Sciences, Vol. 22, No. 2, Feb. 1955, pp. 73-100.

2. Duff, Russell E.: Shock-Tube Performance at Low Initial Pressure. Physics of Fluids, Vol. 1, No. 2, Mar.-Apr. 1959, pp. 207-216.

3. Mirels, Harold: Laminar Boundary Layer Behind Shock Advancing into Stationary Fluid. NACA TN 3401, Mar. 1955.

4. Mirels, Harold: Boundary Layer Behind Shock or Thin Expansion Wave Moving into Stationary Fluid. NACA TN 3712, May 1956.

5. Mirels, Harold: Laminar Boundary Layer Behind a Strong Shock Moving into Air. NASA TN D-291, Feb. 1961.

6. Mirels, Harold; and King, William S.: Series Solution for Shock Tube Laminar Boundary Layer Test Time. AIAA Journal, Vol. 4, No. 5, May 1966, pp. 782-789.

7. Levy, Solomon: Effect of Large Temperature Changes (Including Viscous Heating) Upon Laminar Boundary Layers With Variable Free-Stream Velocity. Journal of the Aeronautical Sciences, July 1954, Vol. 21, No. 7, pp. 459-474.

8. Lees, Lester: Laminar Heat Transfer Over Blunt-Nosed Bodies at Hypersonic Speeds. Jet Propulsion, Apr. 1956, Vol. 26, No. 4, pp. 259-269, 274.

9. Hayes, Wallace D.; and Probstein, Ronald F.: Hypersonic Flow Theory. Academic Press, 1959, pp. 288-316.

10. Martin, W. A.: An Experimental Study of the Boundary Layer Behind a Moving Plane Shock Wave. U. of Toronto UTIA Rep. No. 47, May 1957.

11. Moeckel, Wolfgang E.; and Weston, Kenneth C.: Composition and Thermodynamic Properties of Air in Chemical Equilibrium. NACA TN 4265, 1958.

12. Hansen, C. Frederick: Approximations for the Thermodynamic and Transport Properties of High-Temperature Air. NASA TR-50, 1959.

13. Mirels, Harold: Test Time in Low Pressure Shock Tubes. Aerospace Corp. Rep. No. TDR-169 (3230-12) TN-5, Dec. 27, 1962.

14. Roshko, Anatol: On Flow Duration in Low Pressure Shock Tubes. Physics of Fluids, Vol. 3, No. 6, Nov.-Dec. 1960, pp. 835-842.

15. Bray, K. N. C.: Research in Hypersonic Aerothermodynamics. Department of Aeronautics and Astronautics (Southampton University), A. A. S. U. Rep. No. 251, Feb. 1964.

16. Sandborn, Virgil A.: Measurements of Flow Duration in a Low-Pressure Shock Tube. NASA TN D-1218, 1962.

17. Hartunian, R. A.; Russo, A. L.; and Marrone, P. V.: Boundary-Layer Transition and Heat Transfer in Shock Tubes. Cornell Aeronautical Lab., Inc., Rep. No. AD-1118-A-3, Dec. 1959.

18. Pai, Shih-I: Viscous Flow Theroy, II-Turbulent Flow. D. Van Nostrand Company, 1957, pp. 60-63 and 99-111.

"The aeronautical and space activities of the United States shall be conducted so as to contribute . . . to the expansion of human knowledge of phenomena in the atmosphere and space. The Administration shall provide for the widest practicable and appropriate dissemination of information concerning its activities and the results thereof."

—NATIONAL AERONAUTICS AND SPACE ACT OF 1958

NASA SCIENTIFIC AND TECHNICAL PUBLICATIONS

TECHNICAL REPORTS: Scientific and technical information considered important, complete, and a lasting contribution to existing knowledge.

TECHNICAL NOTES: Information less broad in scope but nevertheless of importance as a contribution to existing knowledge.

TECHNICAL MEMORANDUMS: Information receiving limited distribution because of preliminary data, security classification, or other reasons.

CONTRACTOR REPORTS: Technical information generated in connection with a NASA contract or grant and released under NASA auspices.

TECHNICAL TRANSLATIONS: Information published in a foreign language considered to merit NASA distribution in English.

TECHNICAL REPRINTS: Information derived from NASA activities and initially published in the form of journal articles.

SPECIAL PUBLICATIONS: Information derived from or of value to NASA activities but not necessarily reporting the results of individual NASA-programmed scientific efforts. Publications include conference proceedings, monographs, data compilations, handbooks, sourcebooks, and special bibliographies.

Details on the availability of these publications may be obtained from:

SCIENTIFIC AND TECHNICAL INFORMATION DIVISION

NATIONAL AERONAUTICS AND SPACE ADMINISTRATION

Washington, D.C. 20546